Langmuir

Letter

pubs.acs.org/Langmuir

Atomic Force Microscopy in Viscous Ionic Liquids

Aleksander Labuda and Peter Grütter*

Department of Physics, McGill University, Montreal, Quebec H3A 2T8, Canada

ABSTRACT: Extracting quantitative information from amplitude-modulation atomic force microscopy (AM-AFM) in viscous ionic liquids is difficult because existing theory requires knowledge of the cantilever natural frequency, which cannot be measured in the absence of a resonance peak. We present a new model that describes cantilever dynamics in an overdamped medium ($Q < 0.5$) and derive the theory necessary to extract the stiffness and damping in highly viscous liquids. The proposed methodology is used to measure the solvation layers of an ionic liquid at a gold electrode.

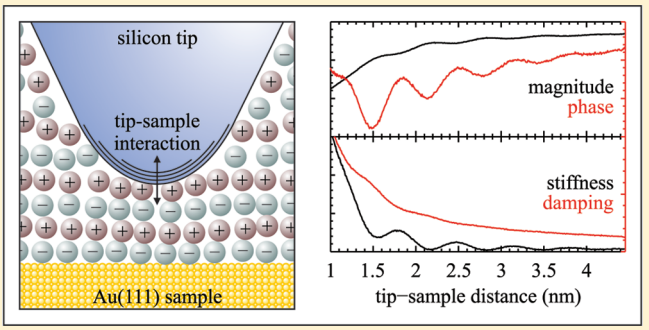

INTRODUCTION

Ionic liquids have recently drawn significant attention for their prospective applications in energy-storage technology,[1,2] organic electronics,[3−5] and nanotribology[6,7] and for their chemical tunability and versatility.[8] By 2007, the culmination of inconsistencies between experiment and theory precipitated a reformulation of electrochemical theoretical foundations based largely on the statistical mechanics of dense Coulomb systems.[9−11] Experimentally, the structure of the electric double layer of ionic liquids is studied by a variety of electrochemical[12−14] and photochemical[15−17] methods, which measure properties averaged over macroscopic or microscopic electrode areas. Atomic force microscopy (AFM) provides a complementary channel of information about the solid−liquid interface, which can be used to verify proposed theoretical models,[18−20] and carries the advantage of probing nanoscopic areas with characterizable electrode roughness and crystallographic orientation. In this respect, AFM results are very relevant for comparison to molecular dynamic simulations,[21,22] which are restricted to nanoscopic volumes with well-defined electrodes.

So far, only static AFM experiments have probed ionic liquid solvation structures at the solid electrode.[23] As an alternative, dynamic amplitude-modulation (AM) AFM[24] provides a direct measure of stiffness and additional damping information (related to the effective viscosity near the surface); however, this technique is overlooked in highly viscous environments because of the lack of a model necessary for extracting physical information from the observed AFM signals. In fact, the resonance peak of a cantilever disappears in highly viscous liquids, preventing the use of existing AM-AFM theory that requires knowledge of the cantilever's natural frequency.

In this letter, we present a new massless model for describing cantilever dynamics in overdamped ($Q < 0.5$) environments, allowing accurate conversion of the amplitude and phase measurements into stiffness and damping signals. We then describe a calibration procedure for overdamped cantilevers based on this massless model and extract the stiffness and damping of solvation layers as a silicon cantilever tip approaches Au(111) in [BMIM][PF_6] (1-butyl-3-methylimidazolium hexafluorophosphate). Finally, the approximations made in deriving the massless model are justified by reference to Sader hydrodynamic theory.[25,26]

THEORY

The first eigenmode of a cantilever can be approximated as a harmonic oscillator that is characterized by mass m, damping γ, and stiffness k, which govern its dynamics by the following differential equation[27]

$$m\ddot{x} + \gamma\dot{x} + kx = f(t) \tag{1}$$

where x is the displacement of the cantilever tip and $f(t)$ is a time-varying force applied to the tip. Taking the Fourier transform leads to a simplified representation

$$C^{-1}(\omega) = \frac{F(\omega)}{X(\omega)} = [k - m\omega^2] + i\omega\gamma \tag{2}$$

where $F(\omega)$ and $X(\omega)$ are the Fourier transforms of force and displacement, respectively. The reciprocal cantilever transfer function $C^{-1}(\omega)$, in units of N/m, will henceforth be referred to as the impedance of the cantilever. This impedance describes the complex-valued restoring force $F(\omega)$ for a given oscillation amplitude $X(\omega)$ as a function of angular frequency ω.

As can be understood from eq 2, the real component of C^{-1} relates to the inertial (conservative) force and the imaginary component represents the viscous (dissipative) force. Both of these components are plotted separately in Figure 1a, and the transfer function $|C|$ is plotted in Figure 1b for reference. In the case of an overdamped cantilever, three distinct harmonic

Received: February 6, 2012
Revised: March 2, 2012
Published: March 4, 2012

   dx.doi.org/10.1021/la300557u | *Langmuir* 2012, 28, 5319−5322

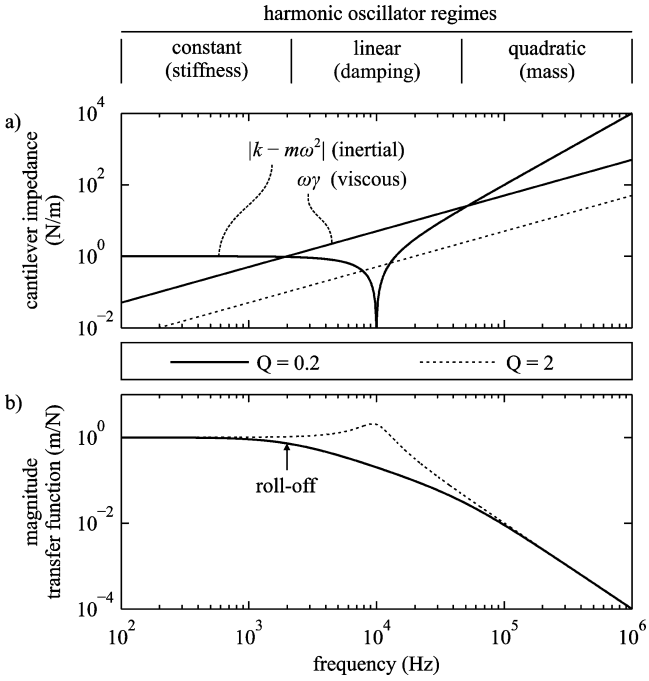

Figure 1. a) Real and imaginary components of the cantilever impedance C^{-1} of an overdamped cantilever (solid lines). Dotted line represents the imaginary impedance of an underdamped cantilever, which is the more familiar case in AFM. b) The corresponding magnitude transfer function $|C|$ is shown for both cases. For an overdamped cantilever, $|C|$ rolls off below the natural frequency and no resonance peak is observed.

oscillator regimes become clear: constant, linear, and quadratic relating to stiffness, damping, and mass, respectively.

Experiments aiming to extract stiffness and damping information should be performed around the intersection of the two first regimes, which coincides with the roll-off frequency of the transfer function $|C|$, as seen in Figure 1. Notice that the impedance C^{-1} up to the roll-off frequency is unaffected by the mass parameter; the inertial component remains nearly constant because $k \gg m\omega^2$. Therefore, mass can be disregarded in overdamped environments when experiments are performed near or below the roll-off frequency, simplifying eq 2 into

$$C^{-1} = k + i\omega\gamma \tag{3}$$

In an experimental setting, the cantilever transfer function C is measured, which can be expressed by its magnitude

$$|C| = \frac{1}{k}\frac{1}{\sqrt{1 + \left(\frac{\omega}{\omega_{ro}}\right)^2}} \tag{4}$$

and phase

$$\theta_C = -\text{atan}\left(\frac{\omega}{\omega_{ro}}\right) \tag{5}$$

This describes a first-order low-pass filter with a roll-off frequency $\omega_{ro} = k/\gamma$.

Note that $C = |C|e^{i\theta_C}$ is in fact the cantilever response measured during an AM-AFM experiment. However, the impedance $C^{-1} = |C|^{-1}e^{-i\theta_C}$ will be used to facilitate the following derivation because inverting C into C^{-1} decouples conservative and dissipative forces into real and imaginary components, respectively, as can be understood from eq 3.

Projecting the complex-valued vector C^{-1} onto real and imaginary axes (using basic trigonometry) provides a convenient way to isolate the stiffness and damping by

$$k = |C|^{-1}\cos\theta_C \tag{6}$$

$$\omega\gamma = -|C|^{-1}\sin\theta_C \tag{7}$$

During the experiment, the stiffness and damping both vary according to tip−sample interactions. Along the real axis, the measured impedance k is the sum of the interaction stiffness k_i and the cantilever stiffness k_c. Along the imaginary axis, the measured impedance is $\omega\gamma$, where γ is the sum of the interaction damping γ_i and the damping γ_s measured at the start of the experiment. This decomposition is illustrated in Figure 2.

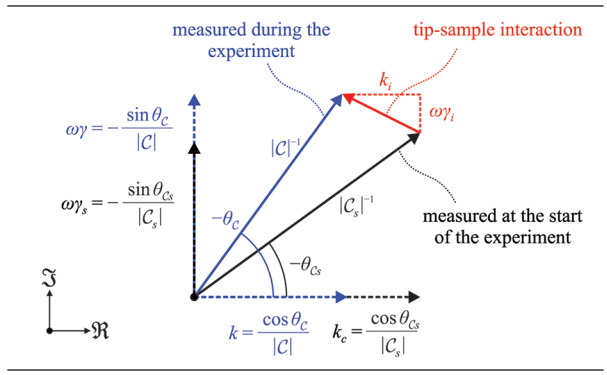

Figure 2. Vector decomposition of the cantilever impedance C^{-1} into inertial ($\mathcal{R}$: real) and viscous ($\mathcal{I}$: imaginary) forces. Simple vector subtraction can be used to extract the tip−sample interaction stiffness and damping.

It follows directly from Figure 2 that the tip−sample interaction stiffness k_i and damping γ_i can be isolated by simple vector subtraction such that

$$k_i = \frac{\cos\theta_C}{|C|} - \frac{\cos\theta_{C_s}}{|C_s|} \tag{8}$$

$$\gamma_i = -\frac{1}{\omega}\left[\frac{\sin\theta_C}{|C|} - \frac{\sin\theta_{C_s}}{|C_s|}\right] \tag{9}$$

Values carrying a subscript "s" are measured at the start of the experiment, in the absence of tip−sample interaction.

CALIBRATION

To make use of eqs 8 and 9, the cantilever must be calibrated at the start of the experiment.

First, a thermal spectrum in air provides k_c via the Sader method.[28] Second, a thermal spectrum in the viscous environment (close to the surface) provides a measure of γ_s directly from the roll-off frequency by $\gamma_s = k_c/\omega_{ro}$. Third, the sensitivity (nm/V) of the AFM is deduced from the fluctuation−dissipation theorem, which states that the thermal driving force spectrum is $F_T = 4k_BT\gamma_s$; therefore, the measured thermal spectrum converges to $4k_BT\gamma_s/k_c^2$ at low frequencies (disregarding additional $1/f$ noise), providing calibrated physical units of fm^2/Hz.

dx.doi.org/10.1021/la300557u | Langmuir 2012, 28, 5319−5322

Note that the second and third steps can be performed simultaneously by fitting the following function to the measured thermal spectrum

$$F_T \times |C|^2 = \frac{4k_BT}{k_c\omega_{ro}} \frac{1}{1 + (\omega/\omega_{ro})^2} \quad (10)$$

with sensitivity as a multiplicative fitting parameter.

This calibration procedure was performed in Figure 3. The cantilever k_c = 28.5 N/m was determined from the thermal spectrum in air, and the thermal spectrum in [BMIM][PF_6] established the damping γ_s = 120 μNs/M and calibrated the measurement into physical units.

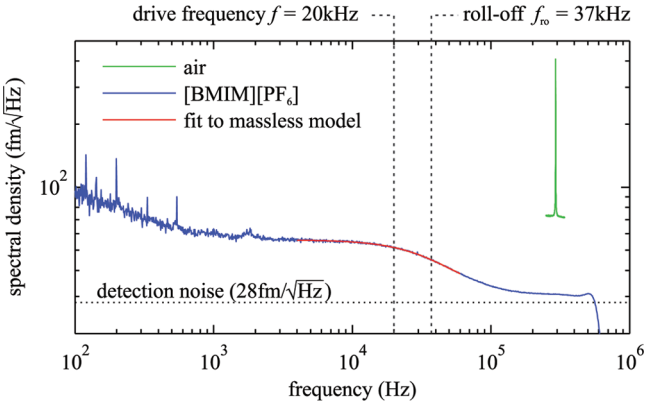

Figure 3. Thermal spectrum in air used to calibrate the cantilever dynamic stiffness k_c = 28.5 N/m. The thermal spectrum in [BMIM][PF_6] was fit using the massless model (eq 10) to extract the roll-off f_{ro} = 37 kHz and to calibrate the plot in units of fm/(Hz)$^{1/2}$. The detection noise was determined independently by acquiring a spectrum at high frequency where the signal is dominated by detection noise rather than thermal noise (not shown).

At this stage, the AFM can be calibrated with respect to any drive frequency chosen for the experiment. The drive frequency was set to 20 kHz, just below the roll-off frequency of 37 kHz, leading to a cantilever magnitude response of $|C_s|$ = 30 pm/nN as calculated by eq 4 and a phase response of θ_{Cs} = −28° as calculated by eq 5.

EXPERIMENT

After 30 min of argon purging, [BMIM][PF_6] was injected into the sealed electrochemical cell on a home-built AFM[29] retrofitted with photothermal excitation.[30] The PPP-NCHAuD cantilever approached the Au(111) surface, followed by the calibration summarized by Figure 3. Photothermally driving the cantilever with an effective 7 nN of force amplitude caused an oscillation amplitude of ∼200 pm at the start of the experiment. Selecting a small amplitude linearizes the measurement,[31,32] thereby facilitating the interpretation of the acquired data. Two hundred continuous approach curves were acquired at an approach speed of 70 nm/s using the spectroscopy module of the Nanonis SPM controller. The magnitude and phase response of the cantilever were measured, as shown in Figure 4a. Equations 8 and 9 were used to extract the tip−sample interaction, plotted in Figure 4b.

An oscillatory stiffness profile is observed, with a period of ∼0.7 nm corresponding to the diameter of a [BMIM][PF_6] ionic pair.[21] The damping, however, is mostly monotonic,[33] with an offset due to squeeze film damping of the cantilever that depends on the tip−sample distance at which the cantilever thermal spectrum was acquired (∼1 μm in this experiment).

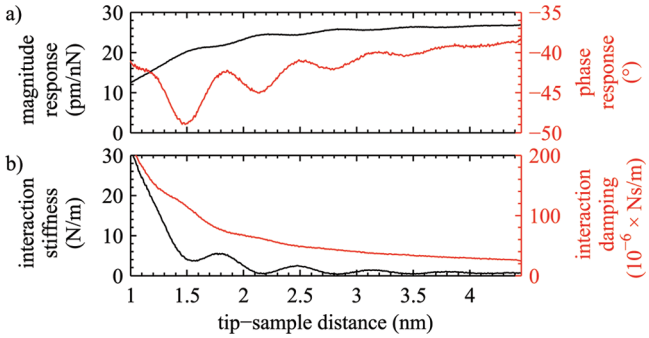

Figure 4. (a) Measured magnitude and phase of the cantilever-transfer function averaged over 200 approach curves in [BMIM][PF_6] on Au(111). Note that the magnitude response is simply the measured amplitude divided by the (constant) driving force of 7 nN. (b) The stiffness and damping profiles are recovered using eqs 8 and 9.

This measurement represents the first step toward quantitative studies of ionic-liquid solvation layers. With an accurate measure of the stiffness and damping profiles, further studies can investigate subtle changes in these profiles as a function of the electrochemical potential in order to extract information about the electric double-layer structure for direct comparison to proposed theoretical models.

JUSTIFICATION OF APPROXIMATIONS

We must justify two noteworthy approximations made in the derivation of the massless model: (1) the damping γ_s is frequency-independent and (2) the mass m is negligible.

On the contrary, the hydrodynamic theory of Sader predicts a frequency-dependent damping for overdamped cantilevers.[25] However, the reviewed theory for cantilevers near rigid walls suggests that damping converges to a constant value as the cantilever−sample distance decreases.[26] As long as the damping is dominated by interaction with a rigid sample, as in our experiment, the approximation of a constant γ_s holds true.

For low Reynolds numbers (<0.1), which are characteristic of overdamped environments, hydrodynamic theory predicts that the effective fluid mass loading of a cantilever decreases as the cantilever approaches the sample.[26] This suggests that the massless approximation of our model is even better than originally expected.

CONCLUSIONS

A massless model, described only by stiffness and damping, suffices to describe the dynamics of an overdamped cantilever up to the roll-off frequency. This simple two-parameter model allows the conversion of phase and amplitude measurements into stiffness and damping for overdamped cantilevers, thereby expanding the capabilities of dynamic AFM to the very low Q regime for quantitative studies of ionic liquids and other highly viscous liquids.

AUTHOR INFORMATION

Corresponding Author

*E-mail: grutter@physics.mcgill.ca

Notes

The authors declare no competing financial interest.

dx.doi.org/10.1021/la300557u | *Langmuir* 2012, 28, 5319−5322

■ ACKNOWLEDGMENTS

We acknowledge fruitful discussions with Yoichi Miyahara, Kei Kobayashi, Martin Lysy, William Paul, and Asylum Research and the generosity of SPECS Surface Nano Analysis Inc., NSERC, FQRNT, and CIfAR.

■ REFERENCES

(1) Conway, B. E. *Electrochemical Supercapacitors*; Plenum Press: New York, 1999.
(2) Simon, P.; Gogotsi, Y. Materials for electrochemical capacitors. *Nat. Mater.* **2008**, *7*, 845−854.
(3) Nakayama, H.; Ye, J.; Ohtani, T.; Fujikawa, Y.; Ando, K.; Iwasa, Y.; Saitoh, E. Electroresistance effect in gold thin film induced by ionic-liquid-gated electric double layer. *Appl. Phys. Express* **2012**, *5*, 023002.
(4) Ono, S.; Miwa, K.; Seki, S.; Takeya, J. A comparative study of organic single-crystal transistors gated with various ionic-liquid electrolytes. *Appl. Phys. Lett.* **2009**, *94*, 063301.
(5) Uemura, T.; Yamagishi, M.; Ono, S.; Takeya, J. Low-voltage operation of n-type organic field-effect transistors with ionic liquid. *Appl. Phys. Lett.* **2009**, *95*, 103301.
(6) Liu, J.; Li, J.; Yu, B.; Ma, B.; Zhu, Y.; Song, X.; Cao, X.; Yang, W.; Zhou, F. Tribological properties of self-assembled monolayers of catecholic imidazolium and the spin-coated films of ionic liquids. *Langmuir* **2011**, *27*, 11324−11331.
(7) Xie, G.; Luo, J.; Guo, D.; Liu, S. Nanoconfined ionic liquids under electric fields. *Appl. Phys. Lett.* **2010**, *96*, 043112.
(8) Hapiot, P.; Lagrost, C. Electrochemical reactivity in room-temperature ionic liquids. *Chem. Rev.* **2008**, *108*, 2238−2264.
(9) Kornyshev, A. Double-layer in ionic liquids: paradigm change? *J. Phys. Chem. B* **2007**, *111*, 5545−5557.
(10) Kilic, M.; Bazant, M.; Ajdari, A. Steric effects in the dynamics of electrolytes at large applied voltages. I. Double-layer charging. *Phys. Rev. E* **2007**, *75*, 1−16.
(11) Oldham, K. B. A Gouy−Chapman−Stern model of the double layer at a (metal)/(ionic liquid) interface. *J. Electroanal. Chem.* **2008**, *613*, 131−138.
(12) Oyama, T.; Yamaguchi, S.; Rahman, M. R.; Okajima, T.; Ohsaka, T.; Oyama, N. EQCM study of the $[Au(III)Cl_4]^-$-$[Au(I)Cl_2]^-$-Au(0) redox system in 1-ethyl-3-methylimidazolium tetrafluoroborate room-temperature ionic liquid. *Langmuir* **2010**, *26*, 9069−9075.
(13) Gnahm, M.; Pajkossy, T.; Kolb, D. M. The interface between Au(111) and an ionic liquid. *Electrochim. Acta* **2010**, *55*, 6212−6217.
(14) Gnahm, M.; Müller, C.; Répánszki, R.; Pajkossy, T.; Kolb, D. M. The interface between Au(100) and 1-butyl-3-methyl-imidazolium-hexafluorophosphate. *Phys. Chem. Chem. Phys.* **2011**, *13*, 11627−11633.
(15) Cremer, T.; Stark, M.; Deyko, A.; Steinrück, H.-P.; Maier, F. Liquid/solid interface of ultrathin ionic liquid films: $[C_1C_1Im][Tf_2N]$ and $[C_8C_1Im][Tf_2N]$ on Au(111). *Langmuir* **2011**, *27*, 3662−3671.
(16) Chang, J.-K.; Lee, M.-T.; Tsai, W.-T.; Deng, M.-J.; Cheng, H.-F.; Sun, I.-W. Pseudocapacitive mechanism of manganese oxide in 1-ethyl-3-methylimidazolium thiocyanate ionic liquid electrolyte studied using X-ray photoelectron spectroscopy. *Langmuir* **2009**, *25*, 11955−11960.
(17) Baldelli, S. Probing electric fields at the ionic liquid-electrode interface using sum frequency generation spectroscopy and electrochemistry. *J. Phys. Chem. B* **2005**, *109*, 13049−13051.
(18) Bazant, M.; Storey, B.; Kornyshev, A. Double layer in ionic liquids: overscreening versus crowding. *Phys. Rev. Lett.* **2011**, *106*, 046102.
(19) Lauw, Y.; Horne, M.; Rodopoulos, T.; Leermakers, F. Room-temperature ionic liquids: excluded volume and ion polarizability effects in the electrical double-layer structure and capacitance. *Phys. Rev. Lett.* **2009**, *103*, 1−4.
(20) Das, S.; Chakraborty, S. Steric-effect-induced enhancement of electrical-double-layer overlapping phenomena. *Phys. Rev. E* **2011**, *84*, 2−5.
(21) Sha, M.; Wu, G.; Dou, Q.; Tang, Z.; Fang, H. Double-layer formation of $[Bmim][PF_6]$ ionic liquid triggered by surface negative charge. *Langmuir* **2010**, *26*, 12667−12672.
(22) Vatamanu, J.; Cao, L.; Borodin, O.; Bedrov, D.; Smith, G. D. On the influence of surface topography on the electric double layer structure and differential capacitance of graphite/ionic liquid interfaces. *J. Phys. Chem Lett* **2011**, *2*, 2267−2272.
(23) Hayes, R.; Borisenko, N.; Tam, M. K.; Howlett, P. C.; Endres, F.; Atkin, R. Double layer structure of ionic liquids at the Au(111) electrode interface: an atomic force microscopy investigation. *J. Phys. Chem C* **2011**, *115*, 6855−6863.
(24) García, R.; Perez, R. Dynamic atomic force microscopy methods. *Surf. Sci. Rep.* **2002**, *47*, 197−301.
(25) Sader, J. E. Frequency response of cantilever beams immersed in viscous fluids with applications to the atomic force microscope. *J. Appl. Phys.* **2008**, *84*, 64.
(26) Green, C. P.; Sader, J. E. Small amplitude oscillations of a thin beam immersed in a viscous fluid near a solid surface. *Phys. Fluids* **2005**, *17*, 073102.
(27) O'Shea, S. J.; Welland, M. E. Atomic force microscopy at solid−liquid interfaces. *Langmuir* **1998**, *14*, 4186−4197.
(28) Sader, J. E.; Chon, J. W. M.; Mulvaney, P. Calibration of rectangular atomic force microscope cantilevers. *Rev. Sci. Instrum.* **1999**, *70*, 3967.
(29) Labuda, A.; Paul, W.; Pietrobon, B.; Lennox, R. B.; Grütter, P. H.; Bennewitz, R. High-resolution friction force microscopy under electrochemical control. *Rev. Sci. Instrum.* **2010**, *81*, 083701.
(30) Labuda, A.; Kobayashi, K.; Kiracofe, D.; Suzuki, K.; Grütter, P. H.; Yamada, H. Comparison of photothermal and piezoacoustic excitation methods for frequency and phase modulation atomic force microscopy in liquid environments. *AIP Adv.* **2011**, *1*, 022136.
(31) Jeffery, S.; Hoffmann, P.; Pethica, J.; Ramanujan, C.; Özer, H.; Oral, A. Direct measurement of molecular stiffness and damping in confined water layers. *Phys. Rev. B* **2004**, *70*, 054114 .
(32) Hofbauer, W.; Ho, R.; Hairulnizam, R.; Gosvami, N.; O'Shea, S. Crystalline structure and squeeze-out dissipation of liquid solvation layers observed by small-amplitude dynamic AFM. *Phys. Rev. B* **2009**, *80*, 134140.
(33) Kaggwa, G. B.; Kilpatrick, J. I.; Sader, J. E.; Jarvis, S. P. Artifact-free dynamic atomic force microscopy reveals monotonic dissipation for a simple confined liquid. *Appl. Phys. Lett.* **2008**, *93*, 011909.